Materials Today Advances 17 (2023) 100353

Contents lists available at ScienceDirect

Materials Today Advances

journal homepage: www.journals.elsevier.com/materials-today-advances/

Nanoparticle biocoating to create ATP-powered swimmers capable of repairing proteins on the fly

Ana Rodríguez-Ramos [a], Miguel A. Ramos-Docampo [b, 1], Verónica Salgueiriño [b, c], Mónica L. Fanarraga [a, *]

[a] Grupo de Nanomedicina-Universidad de Cantabria–IDIVAL Herrera Oria S/n, 39011, Santander, Spain
[b] Departamento de Física Aplicada, Universidade de Vigo, 36310, Vigo, Spain
[c] CINBIO, Universidade de Vigo, 36310, Vigo, Spain

ARTICLE INFO

Article history:
Received 31 October 2022
Received in revised form
22 January 2023
Accepted 24 January 2023
Available online 6 February 2023

Keywords:
Micromotors
Microrobot
Protein repair
ATPase
Chaperone
Heat stress

ABSTRACT

One of the most attractive futuristic challenges in nanomedicine is to create self-propelled nanorobots to scan and repair living tissues at the nano/microscale. Ideally, these devices should navigate using local, inexhaustible biomolecules as energy sources, while performing different functions, such as delivering drugs or repairing tissues.

In this study, we combine nanotechnology and biotechnology to design a biocompatible propulsion system based on the molecular chaperone Hsp90, a *heat-shock protein (Hsp)* that, in the presence of adenosine 5′-triphosphate (ATP), undergoes nanoscale conformational changes while trapping and renaturing other proteins. We show how, subjected to ATP availability in the medium, Hsp90-functionalized particles significantly enhance their diffusion motion, being able to achieve ballistic motion, while keeping the ability to restore the activity of surrounding heat-inactivated proteins. This biomechanics-based propulsion mechanism represents a promising strategy for the design of self-propelled nanodevices capable of performing sophisticated tasks in live biological contexts that include sensing the environment, recognizing and capturing, folding, and restoring defective proteins on the fly. In the short term, Hsp90-driven nanodevices could be applied to improve industrial processes that require enzymatic catalysis and high temperatures. But in the medium to long term, this bioactive coating could be used in the design of nanomachines that, like mini-robots, navigate the complex body cavities of biological tissues, deliver therapies and/or remove misfolded proteins in disorders such as Alzheimer's or Parkinson's disease.

1. Introduction

The design of self-propelled nanomachines capable of targeting specific biomolecular targets has become one of the main challenges in nanobiotechnology. These nanodevices should be able to move *in vivo* indefinitely while performing many other different biological tasks, for example, scanning and detecting damage, repairing the biological tissues, and/or transmitting information as nano-diagnostic systems.

Much progress has been made in achieving micro/nanoscale mobility for these self-propelled devices accomplishing different mechanical movements, such as rotation, rocking, translation, *etc.* [1–8] in response to different specific stimuli [9–11]. The combinations of geometries, sizes, and motion mechanisms explored in the existing literature are virtually endless. The rapidly advancing research in this field has exploited a variety of locomotion mechanisms, often achieving remarkable speeds in diverse environments, ranging from simple aqueous solutions to complex media, including cell cultures or animal tissues.

Active motion has also been triggered by external power sources or by self-propulsion mechanisms using fuel extracted from their surroundings. In most cases, the motility attained takes advantage of magnetic or electric fields, ultrasound, or light [12–19]. Some

Abbreviations: Hsp90, Heat Shock Chaperone 90; ATP, adenosine 5′-triphosphate; FITC, Fluorescein isothiocyanate; IPTG, Isopropyl β-D-thiogalactopyranoside; PS, Polystyrene; SDS-PAGE, Sodium dodecyl sulfate-polyacrylamide gel electrophoresis; GFP, Green fluorescent protein.

* Corresponding author.
E-mail address: fanarrag@unican.es (M.L. Fanarraga).
[1] Miguel A. Ramos-Docampo. Interdisciplinary Nanoscience Center (iNANO), Aarhus University, Gustav Wieds Vej 14, 8000 Aarhus, Denmark.

https://doi.org/10.1016/j.mtadv.2023.100353

devices respond to local temperature [20]; other systems exhibit different mechanisms of motion including self-diffusiophoresis [21,22], self-electrophoresis [23], or bubble-induced propulsion [22], by leveraging energy harvested from different chemicals [24–27]. Among these, a promising alternative to triggering particle movement is to use the intrinsic force generated by catalytic proteins using local molecules as fuel [28–30]. The attached proteins can power swimmers' motion by turnover of their respective substrates through a diffusiophoretic mechanism, stemming from the activity of the number of enzymes adsorbed on their surfaces. The inherent asymmetry in the protein coating while interacting with substrate biomolecules triggers a variable directional movement [31]. Among others, urease, catalase, lipase, DNAse, or glucose oxidase, enhance an induced movement as a consequence of catalysis and substrate substitution, resulting in a form of chemotaxis that responds to the substrate concentration gradient generated by the enzymes themselves [4,13,32–35]. This strategy can be further implemented by coupling the effect of several enzymes that work cooperatively in cascade reactions, amplifying the directional motility of swimmers [28,36,37] that can be enhanced when coupled with magnetic functionality [4].

But so far, all these remarkably interesting approaches have shown little potential translation to the clinic. Among the systems investigated *in vivo,* there are swimmers propelled in intestinal models [38,39] or inside the stomach of living mice [40]. But, while challenges such as crossing the cell membranes to intracellular penetration are still under study [13,41], enzyme-powered devices have opened new exciting opportunities in the design of swimmers driven by physiological substrates.

From a different perspective, it is also possible to attain micro/nanoscale motility by designing biomolecules with intrinsic dynamic functions. The Nobel laureate in Chemistry, B. L. Feringa, pointed out a challenge to program and control molecules by incorporating responsive and adaptive properties, *i.e.,* using their motor functions at the molecular level to design nano-biomachines [42,43]. With very few exceptions, biological movements at the nanoscale (mechanobiology) use adenosine 5′-triphosphate (ATP) as the energy source. The ATP-triggered hydrolysis produces nano-biomolecular conformational changes that ultimately generate mechanical forces, from the protein level -*i.e.* polymerase processing-, to the macroscale -*i.e.* muscle contraction- [44–47]. A paradigmatic example to mention is the rotation motion of the single ATPase protein motors [48] or the amplification of movement from the molecular to the mesoscopic and microscopic level, inducing dynamic changes in the supramolecular organized systems [17]. Thus, ATPases represent a very tempting and even improved alternative to the enzymes used in the design of nano-swimmers, taking into account that, in addition to the molecular biomechanics, ATPases used as propelling nanomotors on particles can also trigger a diffusiophoretic mechanism that, together with the conformational changes, might also contribute to the movement with the conversion of ATP into ADP + Pi.

Some molecular chaperones that are ATPases offer an interesting potential in the design of functional nanoswimmers since they can undergo remarkable conformational changes while counteracting the misfolding of other proteins or preventing the accumulation of toxic aggregates. This is the case of the "heat shock protein" 90 (Hsp90), a highly conserved chaperone that participates in crucial physiological processes and is highly promiscuous, as it interacts with many different client proteins [49]. This molecular chaperone belongs to a family of ubiquitous and highly conserved proteins that are essential in many physiological processes of polypeptide folding/refolding, critical after different types of stress. Most studies show that Hsps can reduce the levels of misfolded proteins *in vitro* and *in vivo*, minimizing the accumulation of aggregates. But what is interesting about Hsp90 is that it behaves like a nanomachine that executes a "clapping" motion while sensing, capturing, and repairing a wide range of "client" proteins in a dynamic ATP-dependent power stroke cycle. (Fig. 1) [50–53]. Focusing on this clapping structural movement, we investigated whether the action of the Hsp90 ATPase can propel nano/microparticles while maintaining its ability to repair misfolded proteins.

2. Results

2.1. Swimmer's design

The first and key step in these swimmers' design is the anchoring of the Hsp90 in a predetermined orientation onto the particles used as substrates. The protein should be placed in such a way that the ATP binding pockets responsible for the clapping movement are oriented peripherally, as sketched in Fig. 1a–c. This would allow the open/close motion of the homodimer to propel the system.

To correctly position and anchor the ATPase protein on the particles, we used an electrostatic method developed in our laboratory (Fig. S1) [54]. This strategy requires modifying the sequence of the Hsp90 protein by attaching a positive peptidic sequence to its carboxyl terminus (Fig. 1b and c). This synthetic cationic tail works as a nanomaterial binding sequence that allows the electrostatic bonding and correct positioning of Hsp90 on the particles. To do this, the 3′of the *hsp90*gene (*htpG*, GENE ID:945,099) was fused to a hexahistidine tag (6xHis) using genetic engineering (Fig. S2a). As a proof of concept, for the swimmer's core, we opted for 500 nm (diameter) carboxylate-modified polystyrene (PS) spheres displaying a ζ-potential value of −45.6 (±0.7) mV in buffer (Table S1, Fig. S2b). The functionalization procedure consisted of incubating the negative particles and the purified protein in a buffer for a few minutes using mild water-bath sonication (Experimental Section, Fig. S1, Table S1). This versatile nanomaterial functionalization strategy allows the binding of the on-purpose engineered proteins to most nanomaterials/nanocomposites displaying a negative ζ-potential (silica particles [54], PS spheres [55], oxidized nanotubes, graphene oxide [56], or gold nanorods [57]), preventing biofouling by surrounding proteins (less than 20% contaminant protein after 72 h incubation at 37 °C). In addition, the bond is very stable, even at extreme physiological pH (5.2–9.0), or when exposed to a wide range of NaCl concentrations (0–1000 mM).[54]. The attachment of the Hsp90 protein to the surface of the PS spheres was confirmed for every particle batch by SDS-PAGE and confocal microscopy (Fig. 1d and e respectively). Theoretical estimation (Table S2) and empirical quantification obtained by thermogravimetric analysis (TGA) (Fig. S3) served to calculate that the number of putative Hsp90 homodimers on the surface of the particles was approximately 60,000–80,000 units per functionalized particle.

To evaluate the functionality of the synthetic Hsp90 protein both, free and bound to PS spheres (PS@Hsp90), we used a luminescent ATP detection kit to quantify the hydrolysis of ATP mediated by the engineered protein. As a negative control, we specifically blocked the ATPase effect using the slow-hydrolyzable ATP competitive inhibitory analog ATPγS (5′-[γ-thio] triphosphate). Fig. S4 demonstrates that neither the genetic changes introduced in the Hsp90 sequence nor the binding of the synthetic protein to the particles interfered with the ATPase activity as represented in the model in Fig. 1a.

PS@Hsp90 particles enhanced Brownian diffusion in the presence of ATP.

Next, we used resonant confocal microscopy for fluorescent particle imaging and tracking analysis. We first investigated

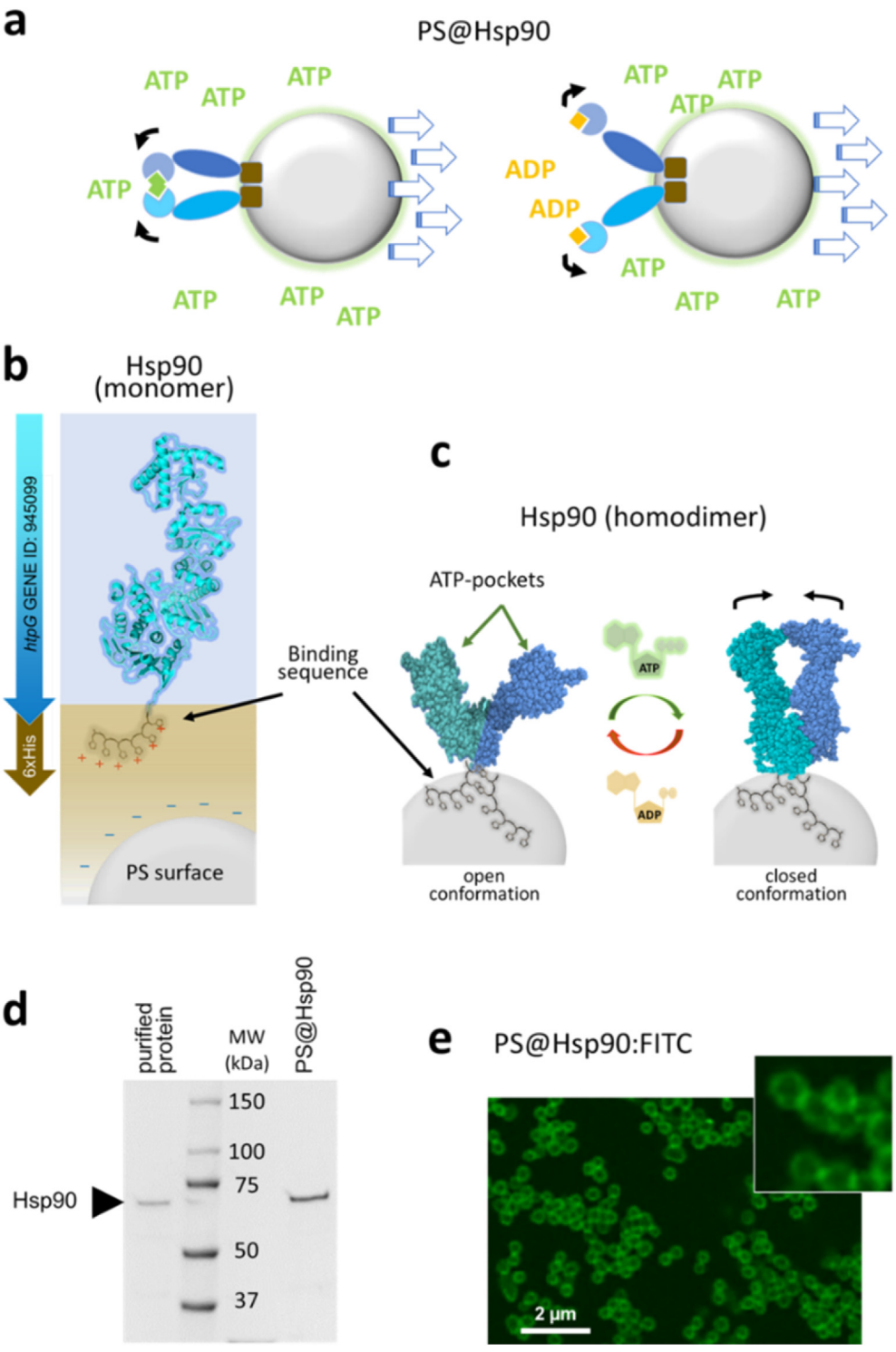

Fig. 1. Hsp90 swimmer design. (a) The amino half of Hsp90 is flexible and can execute a 'clapping' movement hydrolyzing two molecules of ATP in each opening-closing cycle. Two Hsp90 polypeptides (blue) dimerize at the carboxyl terminus (brown) fixed to the PS particle. (b) Structure of the synthetic Hsp90 monomer (blue) attached to the *as-designed* electrostatic binding sequence. (c) Structures of the Hsp90 homodimer during ATP hydrolysis cycle. In the proposed model, the moving parts of Hsp90 are placed peripherally and pointing outwards, leaving the ATP binding pockets fully operational. (d) Coomassie-stained SDS-PAGE gel showing the purified Hsp90 protein used for the coating (left lane) and Hsp90 stripped from the functionalized PS@Hsp90 particles. The central lane shows the molecular weight standards. (e) Confocal microscopy image of the PS@Hsp90:FITC particles. Note: to simplify the diagrams, a single Hsp90 homodimer is drawn. (For interpretation of the references to color in this figure legend, the reader is referred to the Web version of this article).

whether the ATPase activity of Hsp90 could propel PS spheres in the presence of ATP (Video S1). This study permitted quantitative analysis of the movement of PS@Hsp90 particles using the mean-squared displacement (MSD) plotted as a function of short time intervals [58]. In all cases, these MSD plots were computed by averaging all the particles present in the different movie frames and considering no motion in the Z-direction.

We first documented the Brownian behavior of the particles in ultrapure water (Fig. S5a) which, as expected, corresponded to a typical random motion of a colloidal dispersion at a given temperature, in agreement with the linear MSD ($MSD = 4D_{eff}\Delta t$) plot obtained. The diffusion coefficient calculated using the slope of this linear plot was 0.547 (±0.1%) $\mu m^2/s$.

To test our hypothesis, we next documented PS@Hsp90 particle motion in the presence of ATP. The increase in the slope of the MSD plot shown in Fig. S5b revealed that the temperature-dependent Brownian motion transitions to enhanced diffusion [58]. However, as reported previously [4,21,59], due to the averaging of the movement of every particle in all directions, the MSD plots keep exhibiting a linear trend. In this test, the calculated effective diffusion coefficient was 1.299 (±0.1%) $\mu m^2/s$, *i.e.*, twice that of the expected Brownian motion at the given temperature, that is, performing the enhanced diffusion postulated. As a control, PS@Hsp90 particles were also dispersed in water, but in this case, containing the ATPase inhibitor ATPγS (Fig. S5c). As expected, the particles cannot display the enhanced diffusion, but just the Brownian motion, with a calculated diffusion coefficient of 0.536 (±0.1%) $\mu m^2/s$, a value similar to the initial one in the control experiment in ultrapure water.

To rule out nonspecific dragging effects (*i.e.*, sedimentation of the swimmers, or convective currents within the solution) and confirm that the observed movement was dependent on ATP, we then conducted similar experiments mixing the PS@Hsp90 swimmers with identical PS particles coated with a control protein. For this purpose, we functionalized the PS spheres with the green fluorescent protein (GFP), a non-ATPase, as a control protein (Experimental section). A 50:50 (vol: vol) PS@Hsp90: PS@GFP particle mixture was imaged and tracked simultaneously using two fluorescence (red/green) excitation/emission channels to allow a direct comparison of the PS@Hsp90 (red) and PS@GFP (green) spheres under identical conditions.

In the absence of ATP, the MSD plots showed that both particles exhibited Brownian motion caused by random diffusion in the solution, with diffusion coefficients of 0.413 (±1.3%) and 0.477 (±3.1%) $\mu m^2/s$, respectively (Fig. 2a). This means that both protein-coated particles behave similarly under control conditions. However, upon ATP addition, the PS@GFP kept the Brownian motion (with a similar diffusion coefficient of 0.591 (±0.4%) $\mu m^2/s$), but the PS@Hsp90 swimmers presented a linear MSD plot with increased slope, which can be associated to an effectively increased diffusion (with a diffusion coefficient of 1.09 (±2.1%) $\mu m^2/s$). Fig. 2b shows some representative tracked trajectories of the PS@Hsp90 (red) and PS@GFP (green) spheres that reflect indeed the enhanced diffusion in the case of the PS@Hsp90 particles.

To demonstrate that this enhanced motion of the PS@Hsp90 swimmers is triggered because of the presence of the ATP molecules, we added ATPγS to the same sample. The addition of this ATPase blocking agent slowed the PS@Hsp90 swimmers' motion down to random diffusion, becoming comparable to the controls with no ATP. That is, in the presence of ATPγS, the diffusion coefficients of the PS@Hsp90 swimmers dropped to that of the tracer particles, 0.413 (±2.4%) and 0.488 (±0.7%) $\mu m^2/s$, respectively (Brownian diffusion mode).

PS@Hsp90 mobility depends on ATP concentration.

Next, we tested the influence of the concentration of ATP in the PS@Hsp90 particle mobility. To perform this experiment, a 50:50 (vol: vol) PS@Hsp90: PS@GFP particle mixture was imaged and tracked simultaneously at different ATP concentrations (Video S2, Table S3). Fig. 3 displays the calculated MSD plots, traveled distances, and instantaneous velocities, reflecting the performance of the two types of particles in the presence of different ATP concentrations in the media (0, 12, 25, 125 μM). While increasing the concentration of ATP does not affect the dynamics displayed by PS@GFP control particles (showing an average diffusion coefficient of 2.3 (±0.45%) $\mu m^2/s$), PS@Hsp90 particles switch their movement from diffusion (in the absence of ATP) to propulsion (in the presence of ATP), as observed in the MSD plots transitioning from linear to parabolic. Their velocity values increase from 1.9 (±0.13%) μm/s, 2.4 (±0.41%) μm/s, to 3.1 (±0.47%) μm/s), when increasing the concentration of ATP (12, 25, and 125 μM, respectively). To sum up, all these experiments corroborate the hypothesis that the attachment of Hsp90 to particles can significantly increase the mobility stemming from the ATP hydrolysis and validate the PS@Hsp90 as active ATP-powered swimmers.

One plausible mechanism explaining the observed enhanced diffusion motion stems from the conformational changes of Hsp90 powered by ATP hydrolysis [53]. When no ATP is bound, an Hsp90 homodimer adopts a V-shaped, open configuration and undergoes a rather substantial ATP-binding dependent conformational rearrangement that leads to a closed state upon "closure" of the N-terminal domains via intermediate steps (Fig. S4a). After ATP hydrolysis the Hsp90 dimer returns to the open conformation to start another cycle. This opening and closing motion can drive the movement of the particle. Another putative mechanism that could participate is self-diffusiophoresis. This would be caused by the forming concentration gradients of ATP/ADP + Pi in the immediate surroundings of the particle and outwards in the solution when ATP is hydrolyzed. However, contrary to what has been observed for other particles coated with enzymes [4,13,32,33], the Hsp90 dimer hydrolyses ATP at a rate of 0.1–1 per minute [60], and this is quite unlikely to create a concentration gradient of ADP-ATP to move the particle.

Finally, to test whether swimmers could navigate living biological systems (with proteins and other biomolecules in the environment) we repeated the experiments in relevant biological media, in the presence and absence of ATP. For the study, we used serum and human cell extract (see Experimental section). As in the previous cases, PS@Hsp90 and PS@GFP control particles were combined in these media for simultaneous imaging (Video S3). Fig. S6 shows how, in the presence of ATP, PS@Hsp90 swimmers diffuse faster in the serum, reaching a velocity value up to 3 μm/s, but maintain the Brownian and enhanced diffusion regime in the absence of ATP or when immersed in the cell extract medium. Thus, while in the serum the behavior of the particles is very similar to that of water or buffer, in the cell extract a clear slowdown in the velocities of the two types of particles is observed, with and without ATP. We hypothesize that this is due to the different contents and nature of the two biological media. The serum is a homogeneous solution of biomolecules devoid of micro/mesometric bio-particles. But, on the contrary, the post-nuclear cell extract (Experimental Section) contains a high density of biomolecules (that represents about 40% of the cellular volume and a high density of nanometric-scale organelles and nucleic acids) that can significantly interfere with the particle displacement. This result suggests: (i) that the swimmers present a different diffusion/velocity mobility depending on the environment and, (ii) that the mechanisms designed for swimmers should be revised at the intracellular level, where the macromolecular density is very high and there are abundant nano-mesometric structures that could interfere with their movement.

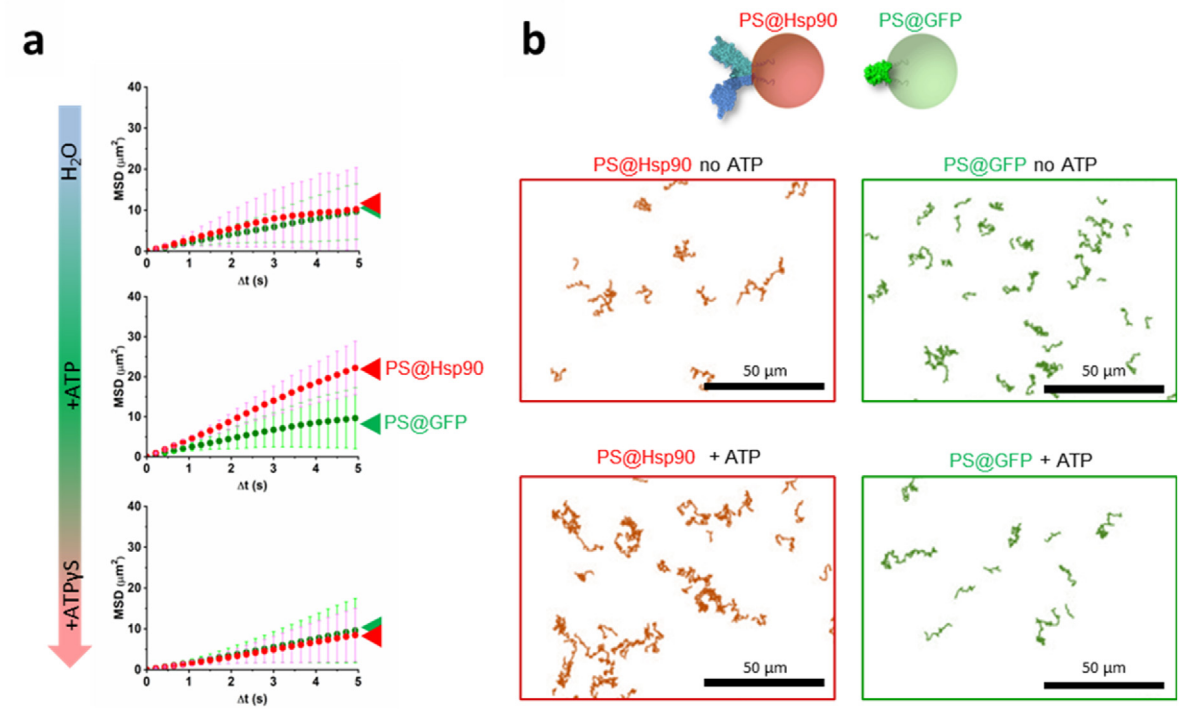

Fig. 2. MSD quantification for PS@Hsp90 and control PS@GFP particles imaged simultaneously. The two types of particles were mixed and resuspended for simultaneous recording (Video S2). (a) MSD of the particles in H_2O (top), and upon sequential addition of ATP (middle), and ATPγS (bottom) to the sample. ATP addition triggers a significant mobility-enhancing effect on PS@Hsp90 particles, while the addition of the blocking agent ATPγS reverses this effect (bottom). PS@GFP particles are not affected by the addition of ATP or ATPγS. (b) Representative tracking trajectories of PS@Hsp90 swimmers and control PS@GFP particles without/with ATP were recorded simultaneously. For clarity, the trajectories of the two-color channels have been separated. (For interpretation of the references to color in this figure legend, the reader is referred to the Web version of this article).

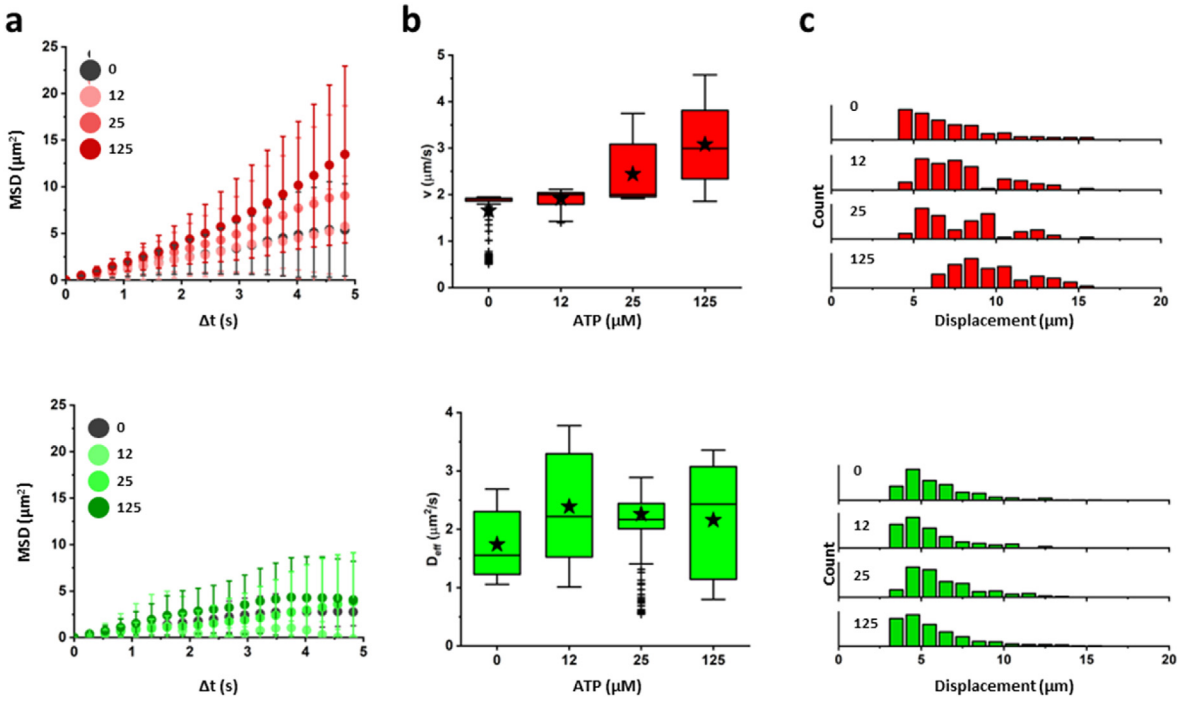

Fig. 3. ATP effect on the swimmers mobility. (a) MSD plot of the PS@Hsp90 (red) and control PS@GFP (green) tracer particles recorded simultaneously in the same sample (Video S2). Circles indicate the ATP concentration. (b) Corresponding whisker plots of the estimated average velocities from PS@Hsp90 (red), and diffusion coefficient of control PS@GFP (green) particles in the presence of different concentrations of ATP. (c) Histograms of the particle traveled distance at the indicated ATP concentrations. (For interpretation of the references to color in this figure legend, the reader is referred to the Web version of this article).

PS@Hsp90 swimmers recognize, capture, and repair proteins on the fly.

Our final challenge was to investigate whether the PS@Hsp90 swimmers could perform a task on the fly, for example, repairing defective proteins. For the test, we identified a chaperone client protein (trypsin) that we heat-denatured to investigate whether the designed swimmers could prevent its inactivation. Trypsin is an enzyme, native to the digestive system of vertebrates, and is a natural protease that digests other proteins into smaller fragments. This enzyme is of notable interest in industrial food processing to improve both the functional and nutritional quality of dietary proteins. As with most proteins, exposure to heat causes trypsin to denature, rendering it fully or partially inactivated. Hsp90, on the other hand, is typically much more resistant to heat stress and can self-renature (‘*Hsp*’ stands for ‘heat shock protein') [61].

To evaluate trypsin activity upon heat stress and further investigate if the PS@Hsp90 swimmers could restore trypsin's function after inactivation, we design a proof-of-concept experiment involving three proteins: a) trypsin, b) Hsp90 (free or attached to the swimmers), and c) a specifically designed trypsin substrate-protein displaying a 25 amino acid ‘tail' that was completely cleaved upon trypsinization (Fig. 4a, S7a, S8). The effective substrate-protein cleavage by trypsin was monitored by SDS-PAGE electrophoresis analysis, where a transition size from ca. 32 kDa (Fig. 4b and c, #1, red arrow) to ca. 27 kDa (#2, green arrow) is observed upon excision (Fig. S7). On the contrary, upon heat inactivation of trypsin (15 min at 90 °C), the protein tag is inefficiently cleavage. This is identified on the gel by the appearance of different protein fragments of sizes between 32 and 27 kD (Fig. 4b and c, #3).

Based on this proof-of-concept model, we tested the swimmers' ability to repair proteins. To do this, trypsin was heat-stressed in the presence of free Hsp90 (as a positive control, Fig. 4b, and c, #4), or of the PS@Hsp90 particles (Fig. 4b and c, #5). The SDS-PAGE analysis of the digestion products of trypsin after these treatments evidenced that both treatments (Fig. 4b and c, #4, #5) preserved almost 100% of the trypsin activity (Fig. 4d, #5).

This study demonstrates that, using ATP as an energy source, these swimmers can (i) sense the environment, (ii) recognize, (iii) capture, and (iv) contribute to the stability and repair of the surrounding proteins. In addition to all this, the results show the great stability of these systems to thermal stress, being able to withstand denaturing conditions for minutes while repairing other proteins. This proof-of-concept study shows the enormous potential of coupling the Hsp90 protein to nano- or mesometric particles. These biosynthetic swimmers could be used in industrial processes, for example, to stabilize expensive catalytic enzymes subjected to high temperatures. The versatility of the system would also allow the assembly of swimmers with magnetic cores or other functionalities that would allow their recovery and recycling after use, thus improving the cost-effectiveness of many industrial biotechnological processes where heat treatment of the products would irreversibly inactivate the expensive enzymes.

3. Discussion

From a general biotechnological perspective, there is huge potential in these Hsp90-based swimmers that can move solely in the presence of ATP. This overcomes one of the biggest problems facing swimmer design, which is finding a propulsion system that uses a fuel that enables ubiquitous, biocompatible biological navigation. The omnipresence of ATP as an energy source, enables the autonomous propulsion of these swimmers in virtually all biological contexts, offering exciting new opportunities in the development of miniaturized tools that access hard-to-reach cavities in the human body to diagnose and treat diseases in a minimally invasive way, or in the field of protein refolding *in vivo*.

Certainly, the speed attained by 500 nm swimmers is not as high as that achieved using other more efficient physicochemical methods, such as light or magnetism. However, these other systems would not be able to navigate indefinitely *in vivo,* where ATP is locally produced and ubiquitous. The swimmer's characteristic enhanced diffusion in the presence of ATP (without the need to increase the temperature of the medium) could be used in many different processes, from the proactive identification of target receptors, to the release and administration of drugs in many different physiological environments. In this sense, the Hsp90-propelled swimmers can easily be implemented for utilities such as movement, tracking, and diagnostic/therapeutic purposes; simply by attaching additional custom-designed proteins (*e.g.,* ligand-proteins) to particles with other intrinsic properties, *e.g.,* magnetic particles. Furthermore, the intrinsic ability of Hsp90 to identify and repair denatured proteins opens the door for the development of biohybrid autonomous nano-devices, capable of navigating the interior of the nervous system while recognizing and repairing amyloidogenic proteins, boosting neural proteostasis to prevent and/or eliminate toxic amyloid aggregation while simultaneously transporting therapeutic compounds.

4. Conclusion

The engineered self-propelled system harnesses protein biomechanics to perform nanoscale tasks with the help of enhanced diffusion. This swimmer is endowed with enormous versatility, allowing a plethora of new designs and customization for each intended application. For example, the motor proteins can be attached to many different nanoparticles (PS, silica, lipid, etc.) which, in turn, can endow it with other functions (drug carriers, imaging systems, etc.). Besides, in addition to the motors, the systems can also be coated with other proteins or ligands to improve their targeting properties or achieve many complementary functionalities. From a basic perspective, these results might represent a major leap in the design of nanorobots, capable of diffusing faster -for example in biological fluids where ATP is available-while counteracting denaturation conditions for other surrounding damaged proteins that would be recognized, captured, and restored by the swimmer simultaneously.

5. Experimental section

Gene synthesis, protein expression, and purification: Synthetic chimera recombinant 6xHis fusion gene constructs encoding the bacterial Hsp90 chaperone (*htpG* GENE ID:945,099) (Fig. S1) genetically fused to a 6-histidine tag (6xHis) at its carboxy-terminus. A GFP His-tagged construct was used as a control and as a reporting protein. Gene constructs were synthesized by General Biosystems, Inc. (Morrisville, USA) and were cloned in pET 15 b plasmid systems (Novagen). One Shot™ BL21 (DE3) *E. coli* (Ref. EC0114, Thermo Fisher Scientific) cells were transformed with the expression vector. Bacterial cultures were grown in Luria-Bertani (LB) broth supplemented with antibiotics (100 μg/mL ampicillin and 35 μg/mL chloramphenicol) until A_{600} *ca.* 0.6. Protein expression was induced by adding 0.5 mM isopropyl β-D-thio-galactopyranoside (IPTG). All proteins were produced and purified in our laboratories following standard biochemical procedures. After protein expression, bacterial pellets were resuspended in 50 mM NaPi, 300 mM NaCl, pH 8.0 with 1 mg/mL lysozyme with protease inhibitor (Pierce, Thermo Fischer Scientific). Cell lysates were obtained by probe sonication. The proteins were purified in Ni-TED columns (Protino® Ni-TED, Macherey-Nagel) following standard protocols. PD-10 Desalting Columns (GE Healthcare) were

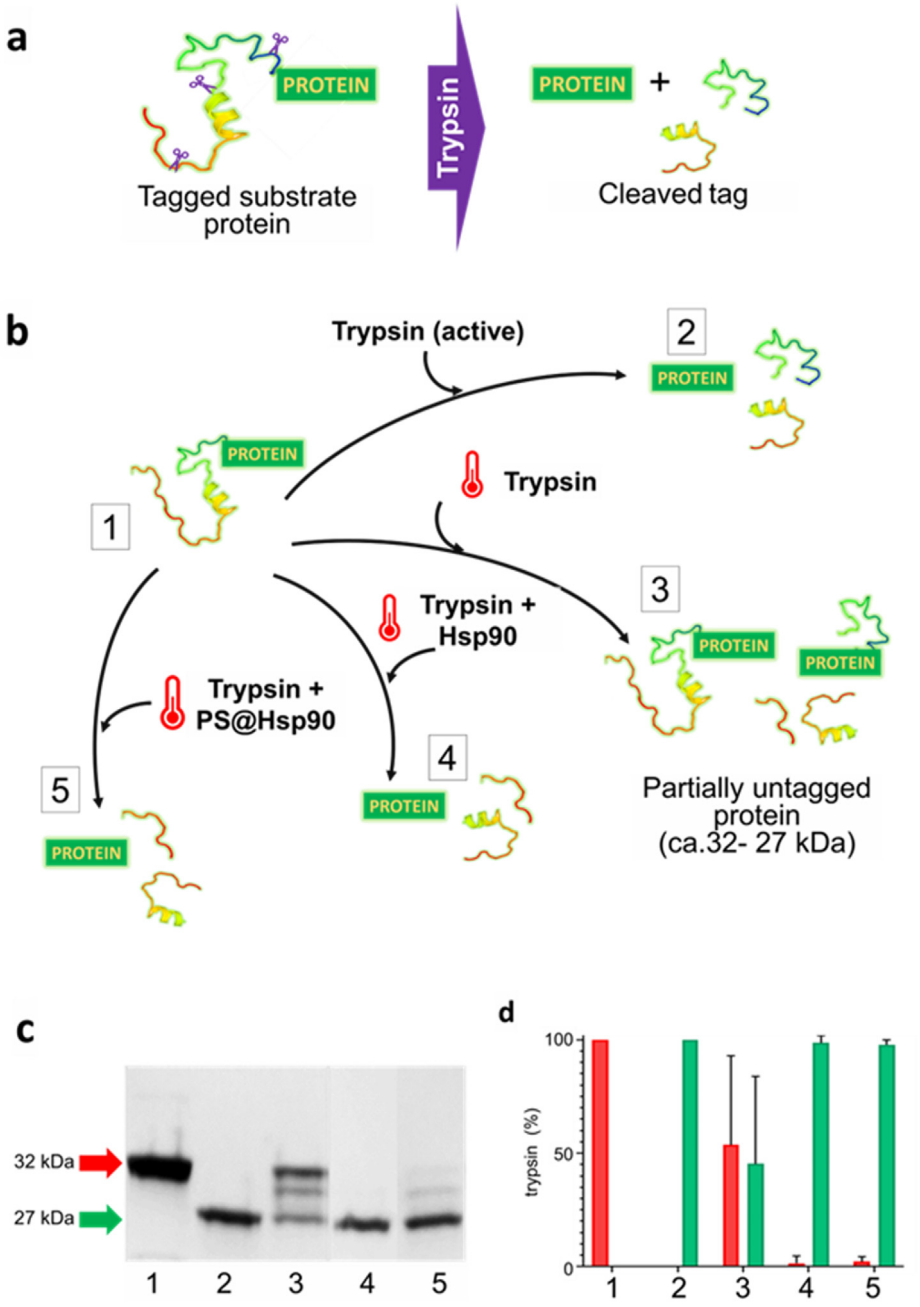

Fig. 4. Evaluation of PS@Hsp90 in the repair of damaged proteins. (a) Proof-of-concept test using trypsin (purple scissors) and a trypsin-cleavable tagged protein. Active trypsin cleaves the tag of the substrate protein. (b) Diagram of tests performed. Efficient trypsin substrate protein digestion (#1) reduces the size of the protein from ca. 32 to ca. 27 kDa (#2). Heat-treated trypsin shows a reduced activity (#3) generating partial intermediate digestion products. Same heat treatments in the presence of free Hsp90 (#4), or PS@Hsp90 swimmers (#5) prevent trypsin denaturation preserving its activity. (c) Trypsin signature analysis using SDS-PAGE analysis. Fig. S8 shows additional biochemical details. Lane numbers correspond to those in the (b) diagram. (d) Quantification of enzyme efficiency after previous treatments. Red/green bars show the amount of uncut/cut (digested) protein respectively. In #4 and #5, trypsin's activity is almost intact. Results are the average quantification of 5 experimental replicas ($n = 5$). Error bars represent *SD*. (For interpretation of the references to color in this figure legend, the reader is referred to the Web version of this article).

used to remove the imidazole and exchange buffer for phosphate-buffered saline (PBS). Protein analysis was performed using SDS-PAGE. Coomasie-stained gels were digitalized and analyzed using the BioRad GelDoc EZ system software.

FITC protein labeling: Purified recombinant Hsp90:6xHis protein was labeled with fluorescein isothiocyanate (FITC, Sigma-Aldrich) in PBS as following standard protocols. Briefly, the protein sample was treated with 1 M sodium bicarbonate buffer, pH 8.8, adding 0.1 mL per 1 mL of protein. Then 50 μL of 5 mg/mL FITC solution in DMSO were slowly added under continuous stirring, and the reaction was kept for 1 h at room temperature. The fluorescently labeled protein was separated from unconjugated FITC by gel filtration (Sephadex® G-25 resin) through a PD-10 column (GE Healthcare).

Swimmer self-assembly and biochemical characterization: Carboxylate-modified latex (PS) white and fluorescent red beads (Sigma-Aldrich, Polysciences, Inc. 09836 and Sigma-Aldrich L3280) of ca. 500 nm diameter were used for functionalization. DLS size

(nm), polydispersity index (PI), and ζ-potential (mV) were all characterized before and after functionalization (Table S1). The particles were functionalized with saturating amounts of the 6xHis-tagged purified protein resuspended in PBS using mild sonication as previously described (Figs. S1 and S2). In brief, 100 μg of particles were immersed in 500 μL PBS containing saturating amounts of the tagged protein (*ca.* 0.5 mg/mL) at room temperature. The mixture was sonicated in a water bath for 5 min. Unbound protein was removed by repeated centrifuge washes (3 washes at 3000 g for 10 min). SDS-PAGE electrophoresis was used to quantify the protein captured on the surfaces of the particles. These were stripped in Laemmli sample buffer (BioRad) at 90 °C. The stripped protein was loaded in precast Mini-Protean® TGX™, BioRad gels for SDS-PAGE analysis. The semi-quantification of the total amount of protein on the surface of the particles was performed on Coomasie-stained gels using the software of the BioRad GelDoc EZ system. We calculated that *ca.* 0.4 μg of recombinant protein was captured per mg of the particles, and approximately 60,000–80,000 homodimers of Hsp90 units/particle (Table S2, Fig. S3).

Transmission electron microscopy (TEM): Functionalized PS particles (10 μL) were resuspended in distilled water and were deposited on a TEM grid (S160-4, agar scientific). Observations were performed on the dried preparations.

To carry out the negative staining process, a 7 μl drop of functionalized PS particles, a 7 μl drop of 2% uranyl acetate, and finally, a drop of water was deposited on a parafilm. The TEM grid (S160-4, agar scientific) was placed upside-down over the drop and incubated for 1 min. Subsequently, it was placed on filter paper and moved to the next drop until the process was complete. Observations were performed on the dried preparations.

Functional assays: A quantification/detection luminescent ATP detection Assay Kit (Abcam) was used to verify recombinant Hsp90:6xHis protein ATPase function both when the chaperone was free in the media or upon binding to the particles. The kit uses a firefly's luciferase that, in the presence of luciferin, produces luminescent oxyluciferin in a quantitative ATP-dependent manner. The amount of magnesium required for ATP binding and hydrolysis with Hsp90s is included in the kit used in the related experiments. For the test, samples of 40 μL of purified recombinant Hsp90:6xHis collected every 90 min, were combined with 40 μL of 0.1 μM ATP in PBS containing 20 μL of the kit's substrate solution in a 96-well plate. Sample luminescence was quantified in a TECAN Spark® luminescent microplate reader.

Mobility tests and confocal image recording: Confocal fluorescent images were taken with a Nikon A1R microscope. Time-lapse fluorescent images of moving particles were acquired using the resonant mode using the 20x lens and were recorded at 15 frames/sec (133.33 msec interval) for 10 min. Scanning was performed using the resonant mode in the two channels dual channels (Ex 488/561 nm; emissions collected at these intervals 500–550 (green) and 570–620 nm (red). Particle tracking was performed using the Nikon NIS-Elements software tracking tools. All fluorescent images are pseudo-colored. Tests were performed directly on a μ-Slide-I Luer (Ibidi) uncoated slide directly on the stage of a Nikon A1R confocal microscope. The fluorescent red PS particles were functionalized with Hsp90:6xHis. For the experiments in Figs. 2 and 3, identical particles with no fluorescence were functionalized in parallel with 6xHis:GFP. The GFP-coated particles, used to normalize and discard the Brownian motion, were imaged simultaneously. Coated particles were dispersed in 100 μL of ultrapure water, added to the microscope slide, and allowed to stabilize for 5 min. Video images were captured upon the addition of 50 μL of 50 μM ATP or ATPγS. The trajectories of the individual swimmers were software-tracked using the Fiji plugin "TrackMate" [62]. These were extracted and imported into Matlab, in which the mean squared displacement (MSD) analyses were performed, as described before [21]. The effective diffusion coefficient (D_{eff}) of swimmers exhibiting random (Brownian) motion was calculated from the slope of the linear fit, according to $MSD = 4D_{eff}\,\Delta t$. The diffusion coefficients are expressed as the average plus/minus the coefficient of variation over the whole ensemble of swimmers in a particular experiment. Given the turbulent-to-stationary regime, the transition is expected to take place, the MSD was plotted within a few seconds of mixing the particles with the ATP solution. During this short period, the temperature in the solution can increase by 1–2 °C, thus contributing to a rise in the average diffusion coefficients in all experiments. In Fig. 3b, whisker plots were employed to represent either the average velocity or the diffusion coefficient of the swimmers. Whisker plots (or boxplots) represent the 1st and 3rd quartiles of the population (upper and lower edges of the box), the median (line crossing each box), and the average (star). Outliers are indicated as crosses. Particle mobility in relevant media was performed in 30% fetal bovine serum (FBS) in medium or 50:50 cell extract/medium; with/without added ATP in both cases. Cell extract was obtained from HEK293 cells. Cells (80% confluent) were detached with media and were sonicated (Sonics Vibra cell VCX130 – tip CV18) with a fine tip (10 pulses of 2 s, amplitude 70%). For the study, the post nuclear cell extract was obtained after centrifugation at 13,400 rpm for 5 min.

Trypsin signature analysis for evaluation of protein heat-denaturation and repair: Trypsin (Gibco, Thermo Fisher Scientific) denaturation was performed at 90 °C for 15 min in PBS. Enzyme function evaluation was performed using an on-purpose designed tagged GFP as a substrate client protein (please see diagram in Fig. S5). Trypsinization was carried out at room temperature for 5 min. Trypsin cleavage SDS-PAGE analysis of the designed client protein produced a ca. 6 kDa polypeptidic chain size reduction (from ca. of approx. 33 kDa to ca. 27 kDa). The swimmer's effect on protein refolding was investigated by incubating the Hsp90-coated particles with the above mixture during the heat denaturation process at 90 °C in the presence of 5 μM ATP (Sigma-Aldrich). Protein was quantified on Coomassie-stained gels and was performed using the BioRad GelDoc EZ system software.

Statistical analysis: Every experiment in Figs. 2 and 3 was conducted in two/three independent repeats, and at least 20 different particles were analyzed per movie. A one-way ANOVA, 0.05 statistical analysis was used. Fig. 4d shows results that are the average of 5 experimental replicas ($n = 5$). Error bars represent SD.

6. Associated content

Supporting Information: **Tables**: Characterization of the particles; Estimates of the number of Hsp90 homodimers; Effective diffusion coefficient and velocity values; Velocity values of PS@Hsp90/PS@GFP particles in serum or cell extract; **Figures:** Diagram of the bioconjugation strategy; Hsp90:6xHis protein sequence, TEM of the PS particles; Calculation of the number of Hsp90 units/swimmer; Recombinant Hsp90 functional tests; MSD plots of PS@Hsp90 in water; MSD plots of PS@Hsp90 and PS@GFP particles in serum and cell extract; Trypsin cutting sites and signature analysis; **Videos:** PS@Hsp90 particles in DW; PS@Hsp90/PS@GFP particles simultaneously recorded in DW, different ATP concentrations; PS@Hsp90/PS@GFP particles simultaneously recoded in biologically relevant media. All are available free of charge via the Internet at http://pubs.acs.org./

Author contributions

ARR, MARD & MLF, performed the experiments. All authors discussed the results and wrote the manuscript. MLF & VS designed

the experiments and obtained the funding. All authors have given approval for the final version of the manuscript.

Declaration of competing interest

The authors declare that they have no known competing financial interests or personal relationships that could have appeared to influence the work reported in this paper.

Data availability

Data will be made available on request.

Acknowledgments

The authors acknowledge the financial support from the Spanish Instituto de Salud Carlos iii, and the European Union FEDER funds under Projects ref. PI22/00030, PI19/00349, from the Spanish Ministerio de Ciencia e Innovación under project PID2020-119242RB-I00 and the European Union H2020-MSCA-RISE-2019 PEPSA-MATE project. ARR and MARD acknowledge financial support from IDIVAL (PREVAL19/04) and the Xunta de Galicia (2017-ED481A/322) respectively. We also acknowledge IDIVAL projects INNVAL19/12 and INNVAL21/19.

Appendix A. Supplementary data

Supplementary data to this article can be found online at https://doi.org/10.1016/j.mtadv.2023.100353.

References

[1] N. Zoaby, J. Shainsky-Roitman, S. Badarneh, H. Abumanhal, A. Leshansky, S. Yaron, A. Schroeder, J. Contr. Release 10 (2017) 75.
[2] T. Li, J. Li, H. Zhang, X. Chang, W. Song, Y. Hu, G. Shao, E. Sandraz, G. Zhang, L. Li, et al., Small 2 (2016) 6098–6105.
[3] S. Tottori, B.J. Nelson, Small 14 (2018), e1800722.
[4] P.S. Schattling, M.A. Ramos-Docampo, V. Salgueiriño, B. Städler, ACS Nano 11 (2017) 3973–3983.
[5] V. Yadav, W. Duan, P.J. Butler, A. Sen, Annu. Rev. Biophys. 77 (2015).
[6] M. Fernández-Medina, M.A. Ramos-Docampo, O. Hovorka, V. Salgueiriño, B. Städler, Adv. Funct. Mater. 30 (2020), 1908283.
[7] K. Bente, A. Codutti, F. Bachmann, D. Faivre, Small 14 (2018), 1704374.
[8] R. Iino, K. Kinbara, Z. Bryant, Chem. Rev. 120 (2020) 1–4.
[9] M. Guix, C.C. Mayorga-Martinez, A. Merkoc, A. Merkoçi, Chem. Rev. 114 (2014) 6285–6322.
[10] M. Fernández-Medina, M.A. Ramos-Docampo, O. Hovorka, V. Salgueiriño, B. Städler, Adv. Funct. Mater. 30 (2020) 1–17.
[11] S. Schuerle, S. Erni, M. Flink, B.E. Kratochvil, B.J. Nelson, IEEE Trans. Magn. 49 (2013) 321–330.
[12] T. Xu, W. Gao, L.P. Xu, X. Zhang, S. Wang, Adv. Mater. 29 (2017), 1603250.
[13] J. Shao, S. Cao, D.S. Williams, L.K.E.A. Abdelmohsen, J.C.M. Hest, Angew. Chem. 132 (2020) 17066–17073.
[14] R.S.M. Rikken, R.J.M. Nolte, J.C. Maan, J.C.M. Van Hest, D.A. Wilson, P.C.M. Christianen, Soft Matter 10 (2014) 1295–1308.
[15] S. Fu, D. Fu, D. Xie, L. Liu, B. Chen, Y. Ye, D.A. Wilson, F. Peng, Appl. Mater. Today 26 (2022), 101348.
[16] H. Hess, J. Clemmens, D. Qin, J. Howard, V. Vogel, Nano Lett. 1 (2001) 235–239.
[17] R. Eelkema, M.M. Pollard, N. Katsonis, J. Vicario, D.J. Broer, B.L. Feringa, J. Am. Chem. Soc. 128 (2006) 14397–14407.
[18] J. Zhang, A. Laskar, J. Song, O.E. Shklyaev, F. Mou, J. Guan, A.C. Balazs, A. Sen, ACS Nano 17 (2022) 251–262.
[19] C. Chen, F. Mou, L. Xu, S. Wang, J. Guan, Z. Feng, Q. Wang, L. Kong, W. Li, J. Wang, et al., Adv. Mater. 29 (2017), 1603374.
[20] Y. Tu, F. Peng, X. Sui, Y. Men, P.B. White, J.C.M. Van Hest, D.A. Wilson, Nat. Chem. 9 (2017) 480–486.
[21] M.A. Ramos-Docampo, M. Fernández-Medina, E. Taipaleenmäki, O. Hovorka, V. Salgueirinō, B. Städler, ACS Nano 13 (2019) 12192–12205.
[22] D. Kagan, M.J. Benchimol, J.C. Claussen, E. Chuluun-Erdene, S. Esener, J. Wang, Angew. Chem. Int. Ed. 51 (2012) 7519–7522.
[23] S. Gáspár, Nanoscale 6 (2014) 7757–7763.
[24] A.M. Brooks, M. Tasinkevych, S. Sabrina, D. Velegol, A. Sen, K.J.M. Bishop, Nat. Commun. 10 (2019) 1–9.
[25] F. Mazur, M. Fernández-Medina, N. Gal, O. Hovorka, R. Chandrawati, B. Städler, Langmuir 36 (2020) 7056–7065.
[26] K.M. Reddy, K. Feris, J. Bell, D.G. Wingett, C. Hanley, A. Punnoose, Appl. Phys. Lett. 90 (2007) 10–13.
[27] T.E. Mallouk, Natl. Sci. Rev. 8 (2021).
[28] M. Nijemeisland, L.K.E.A. Abdelmohsen, W.T.S. Huck, D.A. Wilson, J.C.M. Van Hest, ACS Cent. Sci. 2 (2016) 843–849.
[29] Motilal Mathesh, Jiawei Sun, D.A. Wilson, J. Mater. Chem. B 8 (2020) 7319–7334.
[30] S. Ghosh, F. Mohajerani, S. Son, D. Velegol, P.J. Butler, A. Sen, Nano Lett. 19 (2019) 6019–6026.
[31] X. Arqué, A. Romero-Rivera, F. Feixas, T. Patiño, S. Osuna, S. Sánchez, Nat. Commun. 10 (2019) 1–12.
[32] D. Xu, J. Hu, X. Pan, S. Sánchez, X. Yan, X. Ma, ACS Nano 15 (2021) 11543–11554.
[33] Y. Ye, F. Tong, S. Wang, J. Jiang, J. Gao, L. Liu, K. Liu, F. Wang, Z. Wang, J. Ou, et al., Nano Lett. 21 (2021) 8086–8094.
[34] M. Luo, S. Li, J. Wan, C. Yang, B. Chen, J. Guan, Langmuir 36 (2020) 7005–7013.
[35] F. Mou, Q. Xie, J. Liu, S. Che, L. Bahmane, M. You, J. Guan 8 (2021) nwab066.
[36] L.K.E.A. Abdelmohsen, M. Nijemeisland, G.M. Pawar, G.J.A. Janssen, R.J.M. Nolte, J.C.M. Van Hest, D.A. Wilson, ACS Nano 10 (2016) 2652–2660.
[37] J.R. Howse, R.A.L. Jones, A.J. Ryan, T. Gough, R. Vafabakhsh, R. Golestanian, Phys. Rev. Lett. 99 (2007) 3–6.
[38] S.K. Srivastava, G. Clergeaud, T.L. Andresen, A. Boisen, Adv. Drug Deliv. Rev. 138 (2019) 41–55.
[39] J. Li, S. Thamphiwatana, W. Liu, B. Esteban-Fernández De Ávila, P. Angsantikul, E. Sandraz, J. Wang, T. Xu, F. Soto, V. Ramez, et al., ACS Nano 10 (2016) 9536–9542.
[40] A.C. Hortelao, C. Simó, M. Guix, S. Guallar-Garrido, E. Julián, D. Vilela, L. Rejc, P. Ramos-Cabrer, U. Cossío, V. Gómez-Vallejo, et al., Sci. Robot. 6 (2021), eabd2823.
[41] W. Wang, Z. Wu, Q. He, View 1 (2020), 20200005.
[42] B.L. Feringa, Angew. Chem. Int. Ed. 56 (2017) 11060–11078.
[43] K.Y. Chen, O. Ivashenko, G.T. Carroll, J. Robertus, J.C.M. Kistemaker, G. London, W.R. Browne, P. Rudolf, B.L. Feringa, J. Am. Chem. Soc. 136 (2014) 3219–3224.
[44] C.F. Higgins, K.J. Linton, Nat. Struct. Mol. Biol. 11 (2004) 918–926.
[45] S. Rice, A.W. Lin, D. Safer, C.L. Hart, N. Naber, B.O. Carragher, S.M. Cain, E. Pechatnikova, E.M. Wilson-Kubalek, M. Whittaker, et al., Nature 402 (1999) 778–784.
[46] M.P. Mayer, Mol. Cell 39 (2010) 321–331.
[47] R.T. Sauer, T.A. Baker, Annu. Rev. Biochem. 80 (2011) 587–612.
[48] H. Noji, R. Yasuda, M. Yoshida, K. Kinosita, Nature 386120 (1997) 299–302.
[49] F.U. Hartl, M. Hayer-Hartl, Nat. Struct. Mol. Biol. 16 (2009 166 2009) 574–581.
[50] B. Panaretou, C. Prodromou, S.M. Roe, R. O'Brien, J.E. Ladbury, P.W. Piper, L.H. Pearl, EMBO J. 17 (1998) 4829–4836.
[51] K.A. Krukenberg, F. Förster, L.M. Rice, A. Sali, D.A. Agard, Structure 16 (2008) 755–765.
[52] J. Buchner, Trends Biochem. Sci. 24 (1999) 136.
[53] F.H. Schopf, M.M. Biebl, J. Buchner, Nat. Rev. Mol. Cell Biol. 18 (2017) 345–360.
[54] E. Padín-González, E. Navarro-Palomares, L. Valdivia, N. Iturrioz-Rodriguez, M.A. Correa-Duarte, R. Valiente, M.L. Fanarraga, Nanomed. Nanotechnol. Biol. Med. (2020), 102268.
[55] E. Navarro-Palomares, L. García-Hevia, E. Padín-González, M. Bañobre-López, J.C. Villegas, R. Valiente, M.L. Fanarraga, E. Navarro-palomares, L. García-hevia, E. Padín-gonzález, et al., Cancers 13 (2021) 4920.
[56] L. García-Hevia, M. Saramiforoshani, J. Monge, N. Iturrioz-Rodríguez, E. Padín-González, F. González, L. González-Legarreta, J. González, M.L. Fanarraga, J. Nanobiotechnol. 19 (2021) 129.
[57] E. Navarro-Palomares, L. García-Hevia, J. Galán-Vidal, A. Gandarillas, F. García-Reija, A. Sánchez-Iglesias, L.M. Liz-Marzán, R. Valiente, M.L. Fanarraga, Int. J. Nanomed. 17 (2022) 1–14.
[58] G. Dunderdale, S. Ebbens, P. Fairclough, J. Howse, Langmuir 28 (2012) 10997–11006.
[59] A.C. Hortelao, R. Carrascosa, N. Murillo-Cremaes, T. Patino, S. Sánchez, ACS Nano 13 (2019) 429–439.
[60] Y. Jin, R.S. Hoxie, T.O. Street, Protein Sci. 26 (2017) 1206–1213.
[61] S. Lindquist, E.A. Craig, Annu. Rev. Genet. 22 (1988) 631–677.
[62] J.Y. Tinevez, N. Perry, J. Schindelin, G.M. Hoopes, G.D. Reynolds, E. Laplantine, S.Y. Bednarek, S.L. Shorte, K.W. Eliceiri, Methods 115 (2017) 80–90.